JACS
JOURNAL OF THE AMERICAN CHEMICAL SOCIETY
Communication
pubs.acs.org/JACS

Strong and Dynamic CO_2 Sorption in a Flexible Porous Framework Possessing Guest Chelating Claws

Pei-Qin Liao,[†] Dong-Dong Zhou,[†] Ai-Xin Zhu,[†,‡] Lu Jiang,[†] Rui-Biao Lin,[†] Jie-Peng Zhang,*[,†] and Xiao-Ming Chen[†]

[†]MOE Key Laboratory of Bioinorganic and Synthetic Chemistry, State Key Laboratory of Optoelectronic Materials and Technologies, School of Chemistry and Chemical Engineering, Sun Yat-Sen University, Guangzhou 510275, China

[‡]Faculty of Chemistry and Chemical Engineering, Yunnan Normal University, Kunming 650092, China

Supporting Information

ABSTRACT: Using a bis-triazolate ligand and tetrahedral Zn(II) ion, we synthesized a flexible porous coordination polymer functionalized with pairs of uncoordinated triazolate N-donors that can be used as guest chelating sites to give very high CO_2 adsorption enthalpy and CO_2/N_2 selectivity. The dynamic CO_2 sorption behavior could be monitored well by single-crystal X-ray diffraction.

Having large surface areas and tunable framework structures, porous coordination polymers (PCPs) have shown great potential for CO_2 capture and separation.[1] Importantly, the host–guest interactions in crystalline PCPs can be visualized at the molecular level by X-ray diffraction (XRD) techniques, enabling further optimization of the adsorption performance. Measuring the crystal structures at different CO_2 loading levels is more valuable, especially for flexible frameworks.[2] However, the crystallinity of PCP crystals is usually degraded after guest adsorption/desorption processes. Also, gas molecules are very labile inside the channel (weak host–guest interactions). Therefore, crystal (especially single-crystal) structures of CO_2-loaded PCPs have rarely been reported.[3]

The pore surface of a PCP can be functionalized with various functional groups, such as aromatic N-heterocycles,[4] aromatic amino groups,[5] open metal sites (OMSs),[6] alkylamines,[7] etc., to tune the CO_2 binding affinity from physical adsorption to chemical absorption. These functional groups can be regarded as monodentate binding sites for CO_2. However, monodentate binding sites are usually associated with either weak binding affinity or low reversibility. For instance, chemical absorption is very powerful, but it is generally difficult to release the CO_2 for recycling. Physical adsorption exhibits good reversibility, but its affinity and selectivity for CO_2 are low.

The cooperation of multiple weak interactions is crucial for many important biological phenomena requiring both strong binding affinity and high reversibility (e.g., carrier-protein-mediated transportation). This strategy may be also applied to CO_2 capture and separation (Scheme 1a). For example, Neaton and co-workers predicted that when an exposed Cu^{2+} site is decorated by one and two adjacent uncoordinated tetrazolate N-donors, the CO_2 adsorption enthalpy can be tuned from 9.7 to 21.7 and further to 34.5 kJ mol^{-1}.[8] However, chelation of a single CO_2 molecule by multiple strongly active sites has not been directly observed in PCPs, probably because of the instability of such framework structures (Scheme 1b) and the difficulty of determining the gas-loaded crystal structures. We have demonstrated that in carefully designed metal azolate frameworks (MAFs), the N-donors on the azolate ligands can be rationally controlled as coordination and guest binding sites.[3e] Herein we report a porous MAF functionalized with suitably arranged, flexible pairs of uncoordinated triazolate N-donors that serve as molecular claws for CO_2, as revealed by gas sorption and single-crystal XRD studies.

Scheme 1. Different Arrangements and Roles of Multiple Strong Adsorption Sites for CO_2 (M = Metal Ion, N = Nitrogen Atom, L = Ligand): (a) Strong CO_2 Binding; (b) Stable Framework Structure

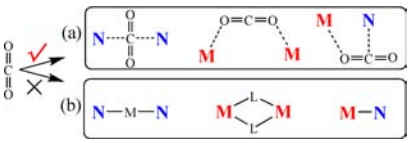

Bis(5-methyl-1*H*-1,2,4-triazol-3-yl)methane (H_2btm) was designed as a chelating–bridging ligand that can coordinate with tetrahedral Zn(II) ions, leaving two triazolate N-donors as guest binding sites. The hydrothermal reaction of $Zn(OH)_2$ and H_2btm in dilute aqueous ammonia gave crystals of $[Zn_2(btm)_2]\cdot 4H_2O$ (MAF-23, $\mathbf{1}\cdot 4H_2O$) in high yield. Microcrystalline $\mathbf{1}\cdot 4H_2O$ was obtained by evaporation of an aqueous ammonia solution of $Zn(OH)_2$ and H_2btm at room temperature.

Single-crystal XRD analysis [Table S1 in the Supporting Information (SI)] revealed that $\mathbf{1}\cdot 4H_2O$ crystallizes in the monoclinic space group $P2_1/n$ with two Zn(II) ions, two deprotonated btm^{2-} ligands, and four H_2O guest molecules in the asymmetric unit (Figure 1 and Figure S1 in the SI). Each Zn(II) ion is tetrahedrally coordinated by four N atoms from three btm^{2-} ligands, and each btm^{2-} ligand coordinates to three Zn^{2+} ions in a bisimidazolate mode, giving a three-dimensional (3D) coordination framework (Figure S2) with 1D narrow channels (void volume 23.4%). As expected, each triazolate ring uses only two N atoms for coordination, leaving the third N atom as a guest binding site. As shown in Figure 1a, four

Received: July 26, 2012
Published: October 8, 2012

dx.doi.org/10.1021/ja3073512 | J. Am. Chem. Soc. 2012, 134, 17380–17383

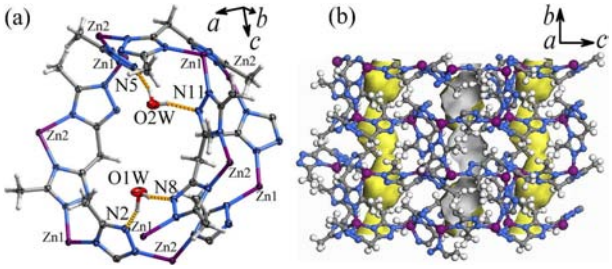

Figure 1. Perspective views of $1{\cdot}4H_2O$: (a) local coordination and hydrogen-bonding interactions (probability ellipsoids drawn at 30%); (b) framework structure (1D channel surface highlighted in yellow; cavity size 7.2 Å × 6.1 Å × 4.9 Å, aperture size 3.6 Å × 3.0 Å).

independent uncoordinated N atoms from four different triazolate rings constitute two pairs of clawlike structures (i.e., N2···N8 and N5···N11), each of which chelates a water molecule via two hydrogen bonds [O···N, 2.821(7)−2.915(4) Å; O−H···N, 153(5)−167(3)°]. Other lattice water molecules (O3W and O4W) are fixed by fewer and weaker hydrogen bonds.

Compound $1{\cdot}4H_2O$ completely retained its crystallinity even after it was refluxed in water for 7 days (Figure S3), which is rare for PCPs.[9] Thermogravimetric analysis (TGA) showed that $1{\cdot}4H_2O$ released all of its water molecules below 150 °C and decomposed above 520 °C (Figure S4). Powder XRD (PXRD) proved that degassed **1** is stable up to 480 °C (Figure S3). The single-crystal structure of **1** was measured to confirm the retention of the host framework and the complete removal of guest molecules (Figure S5). Compared to $1{\cdot}4H_2O$, **1** has a similar unit-cell volume with minor distortions ($\Delta V/V_{1\cdot4H_2O}$ = 0.16%, $\Delta\beta$ = 1.8°). Detailed analysis showed that the structural variation mainly occurred on the coordination bond angles rather than the bond lengths. Dehydration also relaxed the molecular claws [N2···N8 from 5.096(3) to 5.188(3) Å, N5···N11 from 5.434(3) to 5.650(4) Å] because each guest water molecule attracts the two uncoordinated N atoms by hydrogen bonding.

At 195 K, **1** showed a type-I CO_2 sorption isotherm without hysteresis (Figure S6 and Table S2), giving an apparent Langmuir surface area of 622(5) $m^2\ g^{-1}$ and a pore volume of 0.21 $cm^3\ g^{-1}$. The saturated CO_2 uptake was 138 $cm^3\ g^{-1}$, corresponding to 27.2 wt % or 3.0 CO_2 per formula unit; this is higher than the theoretical value (97 $cm^3\ g^{-1}$, 19.0 wt %, 2.0 CO_2 per formula unit) calculated from the crystal structure of **1** using a density of 1.1 g cm^{-3} for liquid CO_2. At 273 and 298 K, **1** showed CO_2 uptakes of 74.2 and 56.1 $cm^3\ g^{-1}$ (i.e., 14.6 and 11.0 wt %), respectively, at 1 atm (Figure 2a and Tables S3−S6). The CO_2 uptake of **1** at 298 K and 1 atm is higher than for

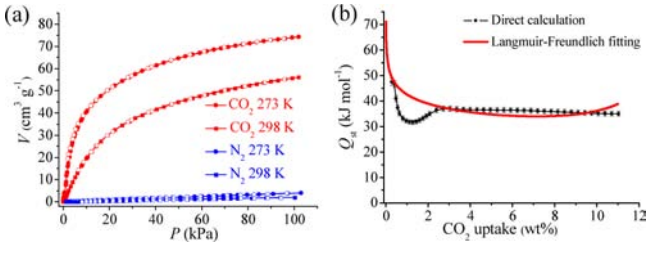

Figure 2. (a) CO_2 and N_2 adsorption (solid) and desorption (open) isotherms and (b) coverage-dependent CO_2 adsorption enthalpy of **1**.

other PCPs with similar or lower surface areas/pore volumes (Table S7).[1c] For N_2 under the same conditions, **1** adsorbs only 4.0 and 2.0 $cm^3\ g^{-1}$ at 1 atm, respectively (Figure 2a and Table S8). Using the initial slopes of the CO_2 and N_2 isotherms, the Henry's law CO_2/N_2 selectivities were calculated to be 163 and 107 at 273 and 298 K, respectively (Figure S7−S8). The CO_2 and N_2 uptakes at the relevant partial pressures for flue gas (0.15 atm CO_2, 0.75 atm N_2) were also calculated to give more practical CO_2/N_2 selectivities of 82 and 87 at 273 and 298 K, respectively. These selectivities are higher than for most PCPs, except for a few functionalized with alkylamines and OMSs.[1c] These observations indicate that **1** can bind CO_2 very strongly. It should be noted that the CO_2 sorption isotherms of **1** are fully reversible and show very fast adsorption/desorption kinetics (Figure S9 and Table S9),[10] indicating that the strong guest adsorption is not necessarily associated with high guest diffusion barriers.

The coverage-dependent CO_2 adsorption enthalpy (Q_{st}) of **1** was calculated with the Clausius−Clapeyron equation using isotherms measured at 273, 283, 290, and 298 K (Figure 2b; also see Figures S10−S14 and Tables S3−S6 and S10−S13). Among various isotherm models, only the Langmuir−Freundlich equation gave fair fits, from which a very high Q_{st} of 71 ± 2 kJ mol^{-1} at zero coverage was obtained. Alternatively, direct calculation without data fitting to any isotherm model gave a near-zero-coverage Q_{st} value of 47.4 ± 1.3 kJ mol^{-1}. Anyway, these values are higher than for PCPs functionalized with uncoordinated azolate N-donors[11] and aromatic amino groups[12] and just lower than for a few PCPs possessing OMSs and alkylamines (Table S14).[6a,7a,b,13] Besides the small pore size, the N···N molecular claw in **1** should be more important for the very high Q_{st}. The direct calculation method should be more reliable than the Langmuir−Freundlich fitting, because the unusual shape of the coverage-dependent Q_{st} profile cannot be described by conventional isotherm models used for rigid adsorbents. As shown in Figure 2b, Q_{st} decreased to a minimum of 31.6 ± 0.8 kJ mol^{-1} at 1.3 wt % and then increased back to 36.9 ± 1.0 kJ mol^{-1} at 2.7 wt %, which can be attributed to framework breathing (decreasing Q_{st}) and guest−guest interactions (increasing Q_{st}). After that, Q_{st} decreased monotonically and slowly to 34.9 ± 0.9 kJ mol^{-1}.

To elucidate the CO_2 adsorption mechanism, single crystals of **1** were fixed inside glass capillaries, activated at 358 K under high vacuum, sealed with back-filled CO_2, and then subjected to XRD at 195 K. The CO_2 loading was controlled by the back-fill pressure and the temperature. A high-quality single-crystal XRD data set was measured for $1{\cdot}1.5CO_2$, in which the gas molecules could be anisotropically refined without any restriction. As shown in Figure 3a, two independent CO_2 molecules reside near the original sites of O1W (denoted as site I) and O2W (denoted as site II). The CO_2 occupancies were determined by free structural refinement to be 0.816(9) and 0.695(10) at sites I and II, respectively. Compared with **1**, the unit cell of $1{\cdot}1.5CO_2$ displays obvious expansion and slight distortion ($\Delta V/V_1$ = 1.4%, $\Delta\beta$ = −0.5°). The CO_2 geometries [C═O, 1.047(14)−1.146(9) Å; O═C═O, 174(2)°] are similar to that of solid CO_2.[14] As expected, each CO_2 is chelated by a molecular claw (i.e., it interacts simultaneously with a pair of uncoordinated N-donors). Most of the N···C separations [N2···C15, 3.011(8) Å; N8···C15, 3.178(8) Å; N5···C16, 3.26(1) Å; N11···C16, 3.15(1) Å] are shorter than the sum of the van der Waals radii of N (1.55 Å) and C (1.70 Å).[15] The N2···C15 distance is significantly shorter than those in all

dx.doi.org/10.1021/ja3073512 | J. Am. Chem. Soc. 2012, 134, 17380−17383

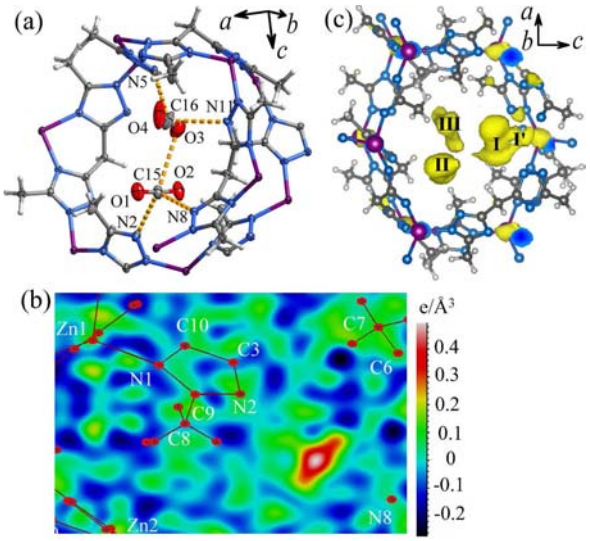

Figure 3. (a) ORTEP plot of the single-crystal X-ray structure of **1**·1.5CO_2 (probability ellipsoids drawn at 30%). (b) 2D difference electron density map ($F_o - F_c$) for **1**·0.07CO_2 showing the presence of CO_2 at site I. (c) 3D electron density map ($F_o - F_c$) of **1**·2.8CO_2 (isosurfaces drawn at 0.60).

previous crystallographic observations (3.14−3.40 Å).[2a,b,3e] The shorter N···C separations and higher CO_2 occupancy of site I indicate that a narrower N···N claw has a higher CO_2 binding affinity. The shortest N···C distance for N2 may be attributed to the different ortho substituents of the uncoordinated N atom (methyl for N2 vs methylene for N5, N8, and N11). Although methyl can induce a stronger $\sigma-\pi$ hyperconjugation effect than methylene,[16] the electron density on the pyridine N atom can be increased by only ca. 2% (from −0.336 to −0.344 electron unit) by methyl substitution at the ortho position.[17] While the pore size of **1**·1.5CO_2 is still very small (cavity size 7.2 Å × 6.5 Å × 4.9 Å, aperture size 3.9 Å × 3.2 Å), the host−guest interactions between other parts of the host framework (methyl and methylene groups) and CO_2 (O atom) are quite weak (Figure S15 and Table S15), further highlighting the significance of the N···N claws. In contrast, there is a significant interaction between the two independent CO_2 molecules [C15···O3, 3.15(1) Å] (Figure 3a).

To visualize further the host−guest interactions at zero coverage, a single crystal was sealed with a very small amount of CO_2 gas, and it showed almost the same unit-cell parameters as for **1** ($\Delta V/V_1$ = 0.01%). The difference electron density map ($F_o - F_c$)[18] showed just one linear three-electron peak at site I (Figure 3b), which was refined as 0.073(5) CO_2 (geometrically restricted), further demonstrating that site I is the strongest CO_2 binding site. The N···C separations in **1**·0.07CO_2 [N2···C15, 2.90(4) Å; N8···C15, 3.00(4) Å] are even shorter than those in **1**·1.5CO_2, confirming that the host−guest interaction is strongest at zero coverage (Figure 2b). One may notice that the host-guest C−H···O interactions have become non-negligible (Figure S16 and Table S16) because the cavity size (7.2 Å × 6.1 Å × 4.9 Å) and aperture size (3.6 Å × 3.0 Å) of **1**·0.07CO_2 are relatively small. However, we must mention that the positions of O atoms are relatively unreliable in the crystal structure of **1**·0.07CO_2.

Since the observed maximum CO_2 uptake was much higher than the theoretical value, structures of CO_2-saturated single crystals were also measured. Unfortunately, the crystals saturated with CO_2 cracked easily, so we obtained only the unit-cell parameters, which were significantly expanded and distorted from those of **1** ($\Delta V/V_1$ = 5.7%, $\Delta\beta$ = −1.7°). Nevertheless, a satisfactory XRD data set was collected for **1**·2.8CO_2, in which not only site I and site II were fully occupied by two CO_2 molecules, but also, another linear three-electron peak (refined as 0.8 CO_2) appeared near the position of O4W in **1**·4H_2O (denoted as site III) (Figure 3c and Figure S17). In **1**·2.8CO_2, the CO_2 molecule at site I was slightly disordered. Besides 0.8 CO_2 (O1═C15═O2) at the original position, there was also 0.2 CO_2 (O1═C15′═O2′) at a nearby position (denoted as site I′), forming closer contacts with the uncoordinated N atoms [C15′···N2, 2.73(4) Å; C15′···N8; 3.04(4) Å] (Figure S18). However, there was also significant steric hindrance from a nearby methyl group [O2′···C8, 2.84(2) Å] (Figure S19). Therefore, CO_2 at site I′ is very labile and can be observed only at low occupancy when the host framework is largely expanded and the CO_2 pressure is high.

Comparison of the crystal structures loaded with different amounts of CO_2 further illustrates the dynamic adsorption behavior of **1**. The unit cell continuously expands and distorts upon adsorption of CO_2 (Figure S20), which can be explained by the flexibility of the host framework and the volumetric effect of the guest. Interestingly, when the CO_2 uptake increases, the N···N and N···C separations of the narrower claw (site I) become wider, while those of the wider claw (site II) become narrower. Near saturated adsorption, the N···N and N···C separations of sites I and II are very similar and even virtually equivalent (Figure 4). These phenomena suggest that

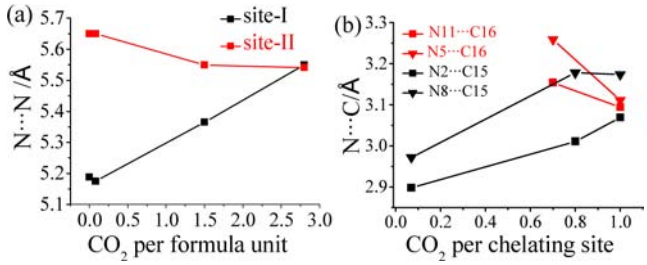

Figure 4. Evolution of the (a) N···N and (b) N···C distances as functions of CO_2 uptake (the lines are drawn to guide the eyes).

as the CO_2 uptake increases, the flexible chelating sites on one hand expand with the host framework but on the other hand shrink because of the convergent attraction of CO_2. The narrower claw mainly expands upon adsorption of CO_2, except at extremely low uptake. For the wider claw, the attraction of CO_2 is more important. When the CO_2 occupancies of sites I and II are equal at saturation, they produce very similar attraction and volumetric effects on the two sites. The almost equivalent N···N and N···C separations of the two sites indicate that the host framework possesses a very high degree of flexibility.

In addition to high robustness/crystallinity of the PCP crystal, precise control over the measurement conditions is very crucial for the determination of single-crystal structures at different gas loading levels. The single-crystal structures of **1**·xCO_2 were measured under the same conditions as for the adsorption isotherm [fixed temperature and varied pressure, i.e., pressure swing adsorption (PSA)], which directly correlates the molecular structure with the adsorption/flexibility properties.

dx.doi.org/10.1021/ja3073512 | J. Am. Chem. Soc. 2012, 134, 17380−17383

Alternatively, fixed pressure and varied temperature [i.e., temperature swing adsorption (TSA)] could be useful for elucidation of sorption isobars. However, constant maintenance of a precise gas pressure for single-crystal XRD study is extremely difficult, except for $P = 0$ (sealing the crystal in vacuum) and $P(N_2) = 1$ atm (open N_2 flow cryostat). To examine the temperature dependence of the framework flexibility, the guest-free single-crystal structures of **1** were also measured at 123 and 298 K (Figure S5). The results revealed moderate thermal expansion coefficients (Figure S21). Since the CO_2 binding affinity of the molecular claw is sensitive to its N···N separation (Figure S22), CO_2 could be strongly captured at a lower temperature and facilely released at a higher temperature, which should make **1** more efficient than conventional rigid adsorbents without such temperature-dependent framework flexibility. The TSA performance of **1** was tested by TGA in a CO_2 flow (Figure 5), which indeed demonstrated very fast sorption kinetics, a relatively low desorption temperature requirement, large working capacity, and good recycling stability.[7]

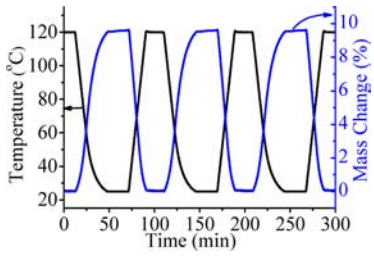

Figure 5. Temperature-cycled TGA of **1** in a CO_2 flow.

In conclusion, we have shown that multiple strong adsorption sites (e.g., uncoordinated azolate N-donors) can be arranged as guest chelating sites, giving strong CO_2 adsorption and high CO_2/N_2 selectivity. Using single-crystal XRD, we also determined the detailed host−guest structures at a fixed temperature with different CO_2 loadings, just as the adsorption isotherm does; this revealed the important roles of the host framework structure and its flexibility.

■ ASSOCIATED CONTENT

Supporting Information

TGA curves, PXRD patterns, additional structural plots, and X-ray crystallographic files in CIF format. This material is available free of charge via the Internet at http://pubs.acs.org.

■ AUTHOR INFORMATION

Corresponding Author

zhangjp7@mail.sysu.edu.cn

Notes

The authors declare no competing financial interest.

■ ACKNOWLEDGMENTS

This work was supported by the 973 Project (2012CB821706) and the National Natural Science Foundation of China (21121061 and 21001120).

■ REFERENCES

(1) (a) Li, J.-R.; Ma, Y.; McCarthy, M. C.; Sculley, J.; Yu, J.; Jeong, H.-K.; Balbuena, P. B.; Zhou, H.-C. *Coord. Chem. Rev.* **2011**, *255*, 1791. (b) Phan, A.; Doonan, C. J.; Uribe-Romo, F. J.; Knobler, C. B.; O'Keeffe, M.; Yaghi, O. M. *Acc. Chem. Res.* **2010**, *43*, 58. (c) Sumida, K.; Rogow, D. L.; Mason, J. A.; McDonald, T. M.; Bloch, E. D.; Herm, Z. R.; Bae, T. H.; Long, J. R. *Chem. Rev.* **2012**, *112*, 724.

(2) (a) Zhang, J.-P.; Chen, X.-M. *J. Am. Chem. Soc.* **2009**, *131*, 5516. (b) Vaidhyanathan, R.; Iremonger, S. S.; Shimizu, G. K.; Boyd, P. G.; Alavi, S.; Woo, T. K. *Science* **2010**, *330*, 650. (c) Queen, W. L.; Brown, C. M.; Britt, D. K.; Zajdel, P.; Hudson, M. R.; Yaghi, O. M. *J. Phys. Chem. C* **2011**, *115*, 24915. (d) Takamizawa, S.; Nataka, E.-i.; Akatsuka, T.; Miyake, R.; Kakizaki, Y.; Takeuchi, H.; Maruta, G.; Takeda, S. *J. Am. Chem. Soc.* **2010**, *132*, 3783. (e) Takamizawa, S.; Takasaki, Y.; Miyake, R. *Chem. Commun.* **2009**, 6625.

(3) (a) Wu, H.; Simmons, J. M.; Srinivas, G.; Zhou, W.; Yildirim, T. *J. Phys. Chem. Lett.* **2010**, *1*, 1946. (b) Tian, Y.-Q.; Zhao, Y.-M.; Xu, H.-J.; Chi, C.-Y. *Inorg. Chem.* **2007**, *46*, 1612. (c) Kim, H.; Kim, Y.; Yoon, M.; Lim, S.; Park, S. M.; Seo, G.; Kim, K. *J. Am. Chem. Soc.* **2010**, *132*, 12200. (d) Maji, T. K.; Mostafa, G.; Matsuda, R.; Kitagawa, S. *J. Am. Chem. Soc.* **2005**, *127*, 17152. (e) Lin, J. B.; Xue, W.; Zhang, J. P.; Chen, X. M. *Chem. Commun.* **2011**, *47*, 926. (f) Wriedt, M.; Sculley, J. P.; Yakovenko, A. A.; Ma, Y.; Halder, G. J.; Balbuena, P. B.; Zhou, H. C. *Angew. Chem., Int. Ed.* **2012**, *51*, 9804.

(4) (a) Lin, J.-B.; Zhang, J.-P.; Chen, X.-M. *J. Am. Chem. Soc.* **2010**, *132*, 6654. (b) Gao, W. Y.; Yan, W.; Cai, R.; Williams, K.; Salas, A.; Wojtas, L.; Shi, X.; Ma, S. *Chem. Commun.* **2012**, *48*, 8898.

(5) (a) Zhao, Y.; Wu, H.; Emge, T. J.; Gong, Q.; Nijem, N.; Chabal, Y. J.; Kong, L.; Langreth, D. C.; Liu, H.; Zeng, H.; Li, J. *Chem.—Eur. J.* **2011**, *17*, 5101. (b) Zhai, Q.-G.; Lin, Q.; Wu, T.; Wang, L.; Zheng, S.-T.; Bu, X.; Feng, P. *Chem. Mater.* **2012**, *24*, 2624.

(6) (a) Dietzel, P. D.; Johnsen, R. E.; Fjellvåg, H.; Bordiga, S.; Groppo, E.; Chavan, S.; Blom, R. *Chem. Commun.* **2008**, 5125. (b) Zhang, Z.; Xiang, S.; Rao, X.; Zheng, Q.; Fronczek, F. R.; Qian, G.; Chen, B. *Chem. Commun.* **2010**, *46*, 7205. (c) Bae, Y.-S.; Farha, O. K.; Spokoyny, A. M.; Mirkin, C. A.; Hupp, J. T.; Snurr, R. Q. *Chem. Commun.* **2008**, 4135.

(7) (a) McDonald, T. M.; Lee, W. R.; Mason, J. A.; Wiers, B. M.; Hong, C. S.; Long, J. R. *J. Am. Chem. Soc.* **2012**, *134*, 7056. (b) McDonald, T. M.; D'Alessandro, D. M.; Krishna, R.; Long, J. R. *Chem. Sci.* **2011**, *2*, 2022. (c) Demessence, A.; D'Alessandro, D. M.; Foo, M. L.; Long, J. R. *J. Am. Chem. Soc.* **2009**, *131*, 8784.

(8) Poloni, R.; Smit, B.; Neaton, J. B. *J. Am. Chem. Soc.* **2012**, *134*, 6714.

(9) Zhu, A.-X.; Lin, R.-B.; Qi, X.-L.; Liu, Y.; Lin, Y.-Y.; Zhang, J.-P.; Chen, X.-M. *Microporous Mesoporous Mater.* **2012**, *157*, 42.

(10) Reid, C. R.; Thomas, K. M. *Langmuir* **1999**, *15*, 3206.

(11) Qin, J.-S.; Du, D.-Y.; Li, W.-L.; Zhang, J.-P.; Li, S.-L.; Su, Z.-M.; Wang, X.-L.; Xu, Q.; Shao, K.-Z.; Lan, Y.-Q. *Chem. Sci.* **2012**, *3*, 2114.

(12) (a) Vaidhyanathan, R.; Iremonger, S. S.; Dawson, K. W.; Shimizu, G. K. *Chem. Commun.* **2009**, 5230. (b) An, J.; Rosi, N. L. *J. Am. Chem. Soc.* **2010**, *132*, 5578. (c) Arstad, B.; Fjellvåg, H.; Kongshaug, K.; Swang, O.; Blom, R. *Adsorption* **2008**, *14*, 755. (d) Si, X.; Jiao, C.; Li, F.; Zhang, J.; Wang, S.; Liu, S.; Li, Z.; Sun, L.; Xu, F.; Gabelica, Z.; Schick, C. *Energy Environ. Sci* **2011**, *4*, 4522. (e) An, J.; Geib, S. J.; Rosi, N. L. *J. Am. Chem. Soc.* **2009**, *132*, 38.

(13) (a) Caskey, S. R.; Wong-Foy, A. G.; Matzger, A. J. *J. Am. Chem. Soc.* **2008**, *130*, 10870. (b) Llewellyn, P. L.; Bourrelly, S.; Serre, C.; Vimont, A.; Daturi, M.; Hamon, L.; De Weireld, G.; Chang, J.-S.; Hong, D.-Y.; Hwang, Y. K.; Jhung, S. H.; Férey, G. *Langmuir* **2008**, *24*, 7245.

(14) Simon, A.; Peters, K. *Acta Crystallogr.* **1980**, *B36*, 2750.

(15) Deguchi, H.; Kubota, Y.; Yagi, Y.; Mitani, I.; Imai, Y.; Tatsumi, M.; Watari, N.; Hirata, T.; Kameda, Y. *Ind. Eng. Chem. Res.* **2010**, *49*, 6.

(16) (a) Fieser, L. F.; Martin, E. L. *J. Am. Chem. Soc.* **1935**, *57*, 1840. (b) Pople, J. A.; Gordon, M. *J. Am. Chem. Soc.* **1967**, *89*, 4253.

(17) Bloor, J. E.; Breen, D. L. *J. Phys. Chem.* **1968**, *72*, 716.

(18) Farrugia, L. *J. Appl. Crystallogr.* **1999**, *32*, 837.